

Allosteric regulation of helicase core activities of the DEAD-box helicase YxiN by RNA binding to its RNA recognition motif

Brighton Samatanga, Alexandra Z. Andreou and Dagmar Klostermeier*

Institute for Physical Chemistry, University of Muenster, Correnstrasse 30, 48149 Muenster, Germany

Received August 03, 2016; Revised December 08, 2016; Editorial Decision December 30, 2016; Accepted January 04, 2017

ABSTRACT

DEAD-box proteins share a structurally similar core of two RecA-like domains (RecA_N and RecA_C) that contain the conserved motifs for ATP-dependent RNA unwinding. In many DEAD-box proteins the helicase core is flanked by ancillary domains. To understand the regulation of the DEAD-box helicase YxiN by its C-terminal RNA recognition motif (RRM), we investigated the effect of RNA binding to the RRM on its position relative to the core, and on core activities. RRM/RNA complex formation substantially shifts the RRM from a position close to the RecA_C to the proximity of RecA_N, independent of RNA contacts with the core. RNA binding to the RRM is communicated to the core, and stimulates ATP hydrolysis and RNA unwinding. The conformational space of the core depends on the identity of the RRM-bound RNA. Allosteric regulation of core activities by RNA-induced movement of ancillary domains may constitute a general regulatory mechanism of DEAD-box protein activity.

INTRODUCTION

DEAD-box RNA helicases remodel RNA secondary structures in an ATP-dependent manner (1–3). Members of this helicase family are composed of a helicase core, formed by N- and C-terminal RecA-like domains (RecA_N, RecA_C) that are connected by a short flexible linker. The core contains the conserved motifs involved in RNA binding, ATP binding and hydrolysis and in the coupling of ATP hydrolysis to unwinding of double-stranded RNA (3–5). In the absence of ligands, the core is in an open conformation, characterized by a large distance between the RecA domains. RecA_N and RecA_C approach each other upon binding of both ATP and RNA, leading to core closure and pro-

moting RNA unwinding (6–9). In addition to the common core, DEAD-box helicases frequently possess flanking regions and ancillary domains that perform diverse functions, including modulation of nucleotide binding and hydrolysis (10,11), specific or unspecific binding of RNAs (12–20), destabilization of the RNA bound to the core (21) and interaction with other binding partners (22). Most structural studies have focused on the helicase core or isolated ancillary domains, and the structural information on full-length helicases is scarce. The underlying mechanisms of how ancillary domains affect helicase function are therefore largely unknown. RNA binding domains may anchor helicases on their target RNAs (18). Yet it is unknown if they act as passive anchors or actively present the bound RNA to the helicase core for unwinding (see (23)). Specifically, it has not been studied if these domains move with respect to the helicase core upon RNA binding, and how RNA binding to the ancillary domain may be communicated to the helicase core.

The *Bacillus subtilis* DEAD-box protein YxiN (Figure 1A) contains an ancillary RNA recognition motif (RRM) C-terminal to its helicase core that specifically binds to hairpin 92 of the 23S ribosomal RNA (rRNA) (16,17,24). Binding of the RRM to this hairpin is thought to anchor YxiN on ribosomal RNA during ribosome biogenesis (24,25). Here, we investigated the mechanism by which the RRM of YxiN affects RNA binding and unwinding, as well as ATP hydrolysis by the helicase core. Using single molecule Förster resonance energy transfer (smFRET), we show that the RRM shifts from a position close to RecA_C in the absence of RNA to a position in proximity of RecA_N when RNA is bound. RNA binding to the RRM alters the conformational space of the helicase core, and stimulates ATP hydrolysis and RNA unwinding. Communication between the RRM and the core is possibly mediated by the short connecting linker that has a high propensity to form α -helical structure. The YxiN RRM is thus not merely a passive anchor but actively modulates the functions of the helicase core.

*To whom correspondence should be addressed. Tel: +49 251 8323421; Fax: +49 251 8329138; Email: dagmar.klostermeier@uni-muenster.de

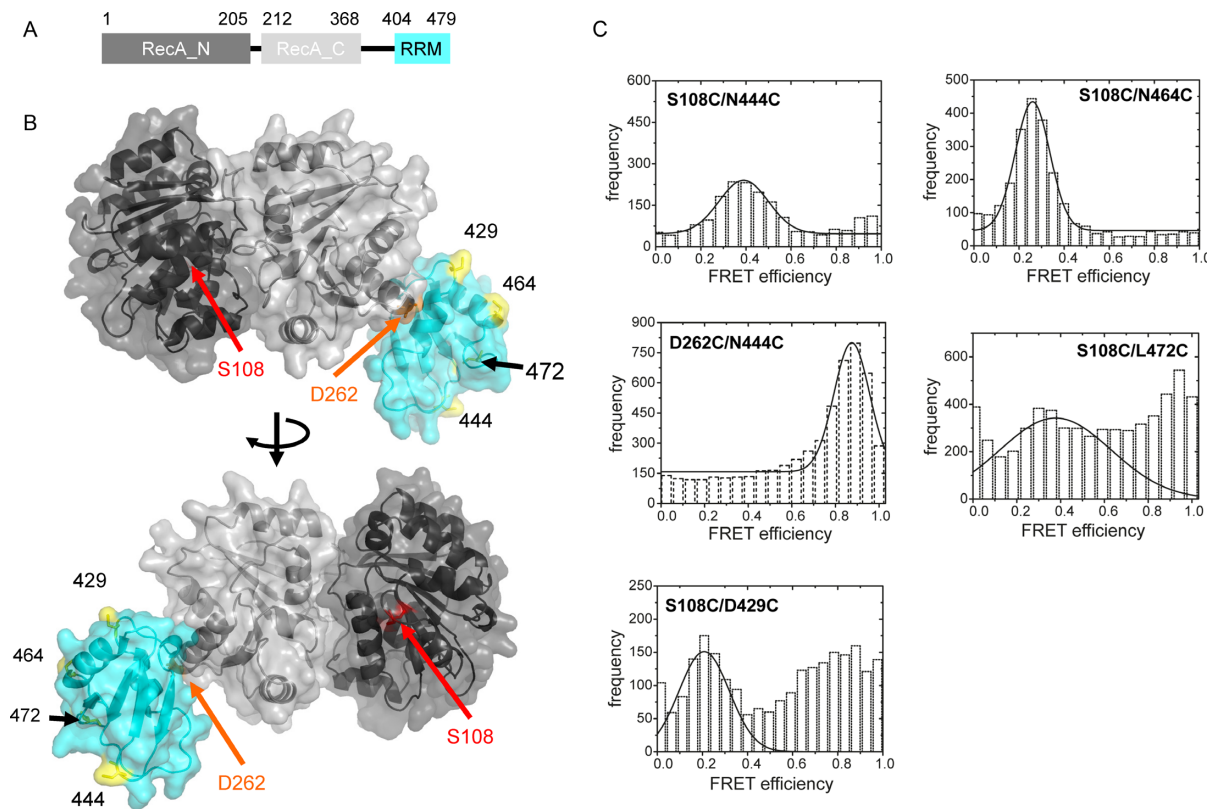


Figure 1. The RRM is located next to the RecA_C in absence of ligands. (A) Domain boundaries of YxiN. RecA_N: N-terminal RecA domain, RecA_C: C-terminal RecA domain, RRM: RNA recognition motif. The numbers indicate the first and last amino acid of each domain. (B) Final YxiN model from FRET-restrained structural modeling. Top: front view, bottom: back view. The YxiN_core (dark gray: RecA_N, light gray: RecA_C) carrying the mutations S108C and D262C in the open state is a homology model, generated using mjDEAD (PDB-ID 1hv8) as a template. The RRM (cyan) containing cysteines at positions 429, 444, 464 and 472, was modeled with the structure of the YxiN RRM (PDB-ID 2goc) as template. Cysteines for fluorophore attachment are numbered and highlighted in yellow. Figures created in PYMOL. (C) Single molecule Förster resonance energy transfer (smFRET) histograms of donor-acceptor-labeled YxiN variants in the absence of RNA. The lines are Gaussian fits to the FRET distributions. The mean E_{FRET} values are summarized in Table 1.

MATERIALS AND METHODS

RNA oligomers

The 32mer, 32merHairpin, 9mer and 15mer, 9merTrap and 14mer RNAs, with or without covalently-linked fluorescein (FAM) or cyanine fluorophores (Cy3 or Cy5), were purchased from Purimex (Grebstein, Germany) in PAGE-purified form or from Axolabs (Kulmbach, Germany) in HPLC-purified form. The sequences are

5'-CGAGGUCCCAAGGGUUGGGCUGUUCGCC CAUU-3' (32mer), 5'-UGGGCUGUUCGCCCAU-3' (32merHairpin), 5'-UUGGGACCU-3' (9mer), 5'-CGAG GUCCCAAGGGU-3' (15mer), 5'- AGGUCCCAA-3' (9merTrap) and 5'-GGGCGGGCCCGCCC-3' (14mer).

The 32mer, 32merHairpin and 14mer RNAs were incubated at 95°C for ~2 min and cooled to room temperature during ~1 h to allow hairpin formation or hybridization. RNA concentrations were determined by UV absorption of denatured RNAs, using the extinction coefficients 298 890 $\text{M}^{-1} \text{cm}^{-1}$ (32mer), 142 560 $\text{M}^{-1} \text{cm}^{-1}$ (32merHairpin) and 206 400 $\text{M}^{-1} \text{cm}^{-1}$ (14mer). The 154mer RNA was produced by *in vitro* transcription using T7 RNA polymerase as previously described (26).

Protein production and purification

YxiN double-cysteine variants for FRET experiments, S108C/D429C, S108C/N444C, S108C/N464C, S108C/L472C, D262C/N444C or S108C/S229C, were produced as GST fusions and purified as previously described (7,9,26). A GST fusion of YxiN_A115C/S229C containing an N-terminal biotinylation tag was co-produced with biotin ligase in the presence of biotin (~40 $\mu\text{g ml}^{-1}$) (27) and purified according to the standard protocol (7,28). All variants are based on the YxiN variant YxiN_C61A_C267A (YxiN) that lacks solvent-accessible cysteines (7,8,29), and have similar secondary structure content and ATP-dependent RNA unwinding activity as the wild-type protein (7,28). The YxiN helicase core (residues 1–368) was produced and purified as previously described (9).

Determination of ATP hydrolysis rates

Rates of ATP hydrolysis were determined under steady-state conditions using an Utraspec 2100pro absorption spectrometer (Amersham Biosciences) and a pyruvate kinase–lactate dehydrogenase enzyme-coupled assay (30) that couples ATP hydrolysis to oxidation of NADH, which

is monitored by the decrease in absorbance at 340 nm wavelength. Measurements were performed with isolated YxiN core and YxiN_S108C/N444C (0.25 μ M) in 50 mM Tris-HCl, pH 7.5, 150 mM NaCl, 5 mM MgCl₂, 2 mM 2-mercaptoethanol in the absence and presence of RNA at 37°C. The reactant concentrations were 5 mM adenosine triphosphate (ATP), 0.2 mM nicotinamide adenine dinucleotide (NADH), 0.4 mM phosphoenolpyruvate, 23 μ g/ml lactate dehydrogenase and 36 μ g/ml pyruvate kinase. RNA concentrations were 5 or 20 μ M 32mer (YxiN_S108C/N444C), 40 μ M of 32mer (YxiN_core), 40 μ M of 32merHairpin RNA (YxiN_S108C/N444C) or 10 μ M of 14-base pair double-stranded RNA.

Fluorescence equilibrium titrations

Steady-state fluorescence anisotropy experiments were conducted on Jobin Yvon (Fluoromax-3 or 4) spectrometers. The dissociation constants (K_d) for YxiN_core-32mer-ADPNP, YxiN_S108C/N444C-32mer or YxiN_S108C/N444C-32merHairpin complexes were determined by titrating the protein to 50 nM (FAM)-32mer-3' or 5'-32merHairpin-(FAM) RNA in 50 mM Tris-HCl, pH 7.5, 150 mM NaCl, 5 mM MgCl₂, 2 mM 2-mercaptoethanol at 25°C. The determination of the K_d value for the YxiN_core/32mer/ADPNP complex was conducted in the presence of 2 mM ADPNP. Fluorescence anisotropy of the fluorescein (FAM) probe was monitored at 520 nm after excitation at 496 nm. K_d values were extracted by describing binding curves according to a 1:1 binding model (Equations 1 and 2):

$$r = r_{\text{free}} + \frac{[YxiN \cdot RNA] \cdot R}{[YxiN \cdot RNA] \cdot R + RNA_{\text{tot}} - [YxiN \cdot RNA]} (r_{\text{bound}} - r_{\text{free}}) \quad (1)$$

with

$$[YxiN \cdot RNA] = \frac{YxiN_{\text{tot}} + K_d + RNA_{\text{tot}}}{\sqrt{\left(\frac{YxiN_{\text{tot}} + K_d + RNA_{\text{tot}}}{2}\right)^2 - YxiN_{\text{tot}} \cdot RNA_{\text{tot}}}} \quad (2)$$

r is the measured anisotropy, r_{free} is the anisotropy of the free RNA, r_{bound} the anisotropy of the bound RNA, R is the change in quantum yield upon binding, $YxiN_{\text{tot}}$ is the total concentration of YxiN and RNA_{tot} is the total RNA concentration.

RNA unwinding experiments

The 32/9mer was prepared by mixing 25 μ M Cy5-32mer-3' with 50 μ M 5'-9mer-Cy3, or by mixing 25 μ M FAM-32mer-3' with 50 μ M 5'-9mer-Cy3. The 15/9mer was prepared by mixing 25 μ M FAM-15mer-3' with 50 μ M 5'-9mer-Cy3. The RNAs were incubated at 95°C for \sim 2 min and cooled to room temperature during \sim 1 h to allow for hybridization. Unlabeled 9merTrap (5 μ M), complementary to the Cy3-labeled 9mer and 5 μ M YxiN core or YxiN_S108C/N444C were added successively to hybridized RNA containing 0.5 μ M Cy5-32mer-3' and 1 μ M 5'-9mer-Cy3 in 50 mM Tris-HCl, pH 7.5, 150 mM NaCl, 5 mM MgCl₂, 2 mM 2-mercaptoethanol at 25°C and unwinding was started by the

addition of 5 mM ATP. The unwinding reaction was monitored by changes in Cy5 acceptor fluorescence at 666 nm after excitation of the Cy3 donor at 554 nm. To investigate the stimulatory function of the 32merHairpin, RNA unwinding of hybridized RNA containing 0.5 μ M FAM-32mer-3' and 1 μ M 5'-9mer-Cy3 or 0.5 μ M FAM-15mer-3' and 1 μ M 5'-9mer-Cy3 by YxiN_N444C in the absence and presence of 5 μ M 32merHairpin was monitored as an increase in fluorescein (FAM) fluorescence at 521 nm after excitation at 495 nm.

smFRET experiments by confocal microscopy

Single molecule FRET experiments of less than 200 pM YxiN (YxiN_C61/A_C261A lacking solvent-accessible cysteines) statistically labeled with AlexaFluor 488 (A488) and AlexaFluor 546 (A546) were conducted on a Microtime 200 confocal microscope (Picoquant, Berlin, Germany) at room temperature in 50 mM Tris-HCl, pH 7.5, 150 mM NaCl, 5 mM MgCl₂, 2 mM 2-mercaptoethanol. smFRET experiments of YxiN/RNA complexes were performed in presence and absence of 5 mM of ADPNP. The RNA concentrations were 1 and 2 μ M 32mer, 5 and 10 μ M 32merHairpin and 0.4 and 2 μ M 154mer RNA. The donor dye was excited at 485 nm. Back-scattered excitation light was rejected by a 505dcXR dichroic mirror, a 100 μ m pinhole and a 532rdc beam splitter. Acceptor and donor emissions were filtered by 570LP or 535/40 bandpass filters, respectively, and detected by SPAD detectors. For the construction of corrected FRET histograms, measured intensities were corrected for differences in quantum yield and detection efficiencies of the detectors, direct excitation of the acceptor dye, leakage of the donor emission into the acceptor channel and leakage of acceptor emission into the donor channel as described (see (31) for details). The quantum yields of the donor labeled YxiN variants were measured relative to fluorescein in 0.1 M NaOH (32,33). Förster distances were determined as described (31). FRET histograms were calculated for each of the two possible donor-acceptor-labeled species: one histogram was generated using correction parameters and Förster distances for the DA-configuration (donor attached to Cys1, acceptor to Cys2), and a second for the inverse AD-configuration (acceptor attached to Cys1, donor to Cys2; Table 1). The two mean FRET efficiencies from these histograms were converted to inter-dye distances r according to Equation (3):

$$r = R_0 \cdot \sqrt[6]{\left(\frac{1}{E_{\text{FRET}}} - 1\right)} \quad (3)$$

where R_0 is the Förster radius (see Table 1). Both distances were used as restraints for rigid-body docking.

FRET-restrained structural modeling

Rigid-body docking iterations of the RRM structure with the homology model of YxiN_core were performed using the FRET-restrained structural modeling software (FPS) (34). The physical dimensions of the dye and dye linkers were explicitly considered: A488 (radius of dye $R_d = 5$ Å, linker length $L_1 = 20$ Å, linker width $L_w = 4.5$ Å) and A546

Table 1. FRET efficiencies, Förster distances and inter-dye distances

Donor	Acceptor	YxiN alone			YxiN/RNA complex		
		E_{FRET}	R_0 (nm)	r (nm)	E_{FRET}	R_0 (nm)	r (nm)
S108C	D429C	0.42	5.8	6.0	N/A	5.6	N/A
D429C	S108C	0.22	5.1	6.3	0.53	4.8	4.7
S108C	N444C	0.40	5.7	6.1	0.53	5.5	5.4
N444C	S108C	0.41	5.1	5.4	0.30	4.7	5.4
S108C	N464C	0.26	5.5	6.6	0.52	5.3	5.2
N464C	S108C	0.39	5.3	5.7	0.56	5.2	5.3
S108C	L472C	0.35	5.4	6.0	0.36	5.1	5.6
L472C	S108C	0.46	5.2	5.3	0.37	4.8	5.3
D262C	N444C	0.88	5.3	3.8	0.58	4.9	4.6
N444C	D262C	0.90	5.2	3.6	0.35	4.9	5.4

E_{FRET} : FRET efficiency, R_0 : Förster distance, r : experimental inter-dye distance, calculated from E_{FRET} for different dye orientations. N/A: could not be determined.

($R_d = 8.1 \text{ \AA}$, $L_l = 20 \text{ \AA}$, $L_w = 4.5 \text{ \AA}$). L_w for Cys 472 was set to 3.5 \AA . A total of 5000 docking iterations were performed starting from a clash tolerance of 6 \AA , through 2.0 to 0.5 \AA , in accordance with previous studies (34). At least 20% (1000 structures) of all the conformers with the lowest chi-squared values were analyzed, in accordance with previous studies (34).

smFRET experiments by TIRF microscopy

TIRF experiments were performed using an Olympus total internal reflection fluorescence (TIRF) microscope as previously described (27). Microscope slides and coverslips were cleaned with 10% alconox (or SDS) and KOH, passivated with polyethylene glycol (PEG) doped with biotinylated PEG, and functionalized by coupling of streptavidin. A total of $0.5 \mu\text{M}$ YxiN RecA_N was added to saturate surfaces and to prevent unspecific binding of YxiN. N-terminal biotinylated YxiN_A115C/S229C in 50 mM Tris-HCl, pH 7.5, 150 mM NaCl, 5 mM MgCl_2 , 2 mM 2-mercaptoethanol was labeled with A555 and A647, immobilized and imaged in the absence and presence of $15 \mu\text{M}$ 32mer, $1 \mu\text{M}$ 154mer and/or 5 mM ADPNP or 20 mM ATP in the presence of oxygen scavenger (5 mM proteocatechuate/100 nM proteocatechuate-3,4-dioxygenase) and triplet state quencher (2 mM Trolox). The time resolution was 150 ms . Trajectories of donor and acceptor intensities were extracted from TIRF movies using an in-house Labview software. The FRET efficiency was calculated from the acceptor I_A and donor intensities I_D , corrected for differences in quantum yield of the dyes and in detection efficiencies (γ , Equation 4) (35).

$$E_{\text{FRET}} = \frac{I_A}{I_A + \gamma I_D} \quad (4)$$

Idealized FRET values were then determined by Hidden Markov Modeling of FRET time traces using vbFRET (36). Transition density plots (TDPs) were calculated as described (37). Fluctuation density plots (FDPs) for molecules that do not change their FRET state during the course of the experiments were created similarly to transition density plots using own Matlab scripts. One of the FRET states was altered by an insignificant 0.0001 units to attain non-zero values in the exponents.

RESULTS

The YxiN RRM is positioned next to RecA_C in the absence of RNA

To investigate whether the RRM moves relative to the helicase core in response to RNA binding, we delineated the positions of the RRM of YxiN relative to the helicase core in both the presence and absence of RNA by performing smFRET experiments on freely diffusing donor-acceptor labeled YxiN using confocal microscopy. YxiN variants with cysteines at either position 108 on RecA_N or position 262 on RecA_C, and at positions 429, 444, 464 or 472 on the RRM (28), were labeled statistically with Alexa488 (donor) or Alexa546 (acceptor; Figure 1A). All cysteine variants unwind a model 32/9mer RNA substrate derived from 23S rRNA comparable to wild-type YxiN (28). smFRET histograms in the absence of RNA, corrected for cross-talk, different quantum yields and detection efficiencies for donor and acceptor and for direct acceptor excitation (31), generally exhibit a unimodal distribution consistent with a defined position of the RRM relative to the core (Figure 1B). The determined FRET efficiencies are in agreement with previous experiments (28). Two variants, S108C/L472C and S108C/D429C, showed an additional peak at high E_{FRET} (>0.7) that is most likely due to aggregation. The tendency to aggregate has been noted previously (28). The high FRET efficiency of 0.7 implies short distances between C108 and C429 or C108 and C472 that are geometrically impossible in combination with the other distance restraints obtained (28). These species were therefore not included in the subsequent analysis. FRET histograms were calculated for D/A and A/D configurations (donor on RecA_N or RecA_C, acceptor on the RRM or *vice versa*), and the mean FRET efficiencies (E_{FRET}) from both analyses were converted into inter-dye distances (Table 1). Both distances were used as a restraint in rigid-body docking of the crystal structure of the free RRM (PDB-ID 2goc) to a homology model of YxiN core, generated by SWISS-MODEL with the structure of mjDEAD (PDB-ID 1hv8) (38) as a template (Figure 1A). The docking procedure was performed with the FRET-restrained Positioning Software (FPS) that takes into account the physical dimensions of the fluorophores (34,39,40). FPS explicitly computes spatial distributions of dye positions, and enables more accurate

and precise determination of the RRM position than previous manual docking attempts (28). Docking iterations were started from 5000 random initial positions of the RRM relative to the core. Convergence was reached in two rounds of positional refinement. Analysis of >20% of the 1000 structures with lowest reduced chi-squared values revealed a set of conformers that converged on a single position of the RRM, in proximity to RecA_C (Figure 1A; Supplementary Figure S1). The molecular shape is in agreement with small angle X-ray scattering results (41), and the structural model is similar to the previously reported one derived from manual docking (28). Thus, the RRM populates a unique position relative to the core, in proximity to RecA_C, in the absence of RNA.

The RRM shifts to a position closer to RecA_N upon RNA binding

To evaluate the effect of RNA binding to the RRM on the overall conformation of YxiN, we performed smFRET experiments in the presence of saturating concentrations of 32mer RNA. The 32mer RNA (Figure 2A) contains hairpin 92 of the 23S rRNA, as well as a 5'-single-stranded extension derived from helix 91 (42), and has been used as a model substrate for YxiN before (7,8,16,17,26,43). Binding of the 32mer led to an increase in E_{FRET} for S108C/N464C, S108C/N444C and S108C/D429C, and a decrease for D262C/N444C (Figure 2A, Table 1). No significant change in E_{FRET} was observed for S108C/L472C. The decrease in E_{FRET} between dyes attached to RecA_C (D262C) and the RRM (N444C) and concomitant increase between dyes attached to RecA_N (S108C) and the RRM (D429C, N464C, N444C) indicates a shift of the RRM away from RecA_C, toward RecA_N. Docking iterations using FPS, with the experimental inter-dye distances (Table 1) as restraints, defined a unique position of the RNA-bound RRM close to RecA_N (Figure 2B). RNA binding thus causes a drastic movement of the RRM relative to the core, with an overall translational movement by 53 Å and a rotation of 37°.

RNA binding to the RRM drives its positional shift

The 32mer contacts the RRM through the hairpin loop (16,17,42), and could in principle interact with the helicase core through the single-stranded extension, raising the question whether RNA binding to the RRM is sufficient to trigger RRM movement, or if simultaneous contacts of the RNA with the core are required. YxiN binds the isolated hairpin of the 32mer (32merHairpin; Figure 2A) lacking the single-stranded extension with a 40-fold lower affinity ($K_d = 7.0 \mu\text{M}$) than the 32mer ($K_d = 0.17 \mu\text{M}$; Figure 3A) (17). This loss in affinity can be attributed to interactions of the RRM with the single-stranded region (17,42). The isolated YxiN core does not bind the 32mer (Figure 3A), neither in the absence nor in the presence of the non-hydrolyzable ATP analog ADPNP that increases the affinity of YxiN for RNA (7,9), supporting that the single-stranded region of the 32mer is not bound by the core. The movement of the RRM upon binding to the 32mer thus seems to originate from the interaction of the RRM with the 32merHairpin. To test this hypothesis, we monitored changes in E_{FRET}

for YxiN_S108C/N444C in the presence of the 32merHairpin RNA. The 32merHairpin induced the same change in E_{FRET} as the 32mer (Figure 4A), suggesting that RNA binding to the RRM provides the energy for RRM movement, without contribution of direct contacts between the RNA and the core. A much larger fragment of the 23S rRNA, the 154mer (7,16,24), influenced the position of the RRM similarly to the 32mer (Figure 4B), indicating that RRM movement is independent of the context in which hairpin 92 is found.

The RRM is required for RNA-induced ATP hydrolysis and RNA unwinding by the YxiN core

We next investigated whether the shift in position of the RRM upon RNA binding affects the functions of the helicase core, and determined rates of ATP hydrolysis in the absence and presence of RNA in an enzyme-coupled assay (30). YxiN (both full-length and core) showed negligible ATPase activity in the absence of RNA (Figure 3B). Upon adding 40 μM of 32mer RNA, the ATPase activity of the isolated core remained negligible, with $k_{\text{hyd}} = 2.4 (\pm 0.4) \cdot 10^{-3} \text{ ATP YxiN}^{-1} \text{ s}^{-1}$, in agreement with its undetectably low 32mer affinity (Figure 3A). The ATPase activity of YxiN increased to $k_{\text{hyd}} = 1.24 \pm 0.04 \text{ ATP YxiN}^{-1} \text{ s}^{-1}$ in the presence of saturating concentrations of 32mer (20 μM), which is in agreement with previous measurements (0.92 s^{-1} ; (17)), and over 500-fold higher than the ATP hydrolysis rate of the core. Interestingly, the 32merHairpin (40 μM) stimulated the ATPase activity to $k_{\text{hyd}} = 0.20 \pm 0.04 \text{ ATP YxiN}^{-1} \text{ s}^{-1}$, which is only 6-fold lower than the activity in presence of the 32mer, suggesting that RNA binding to the RRM stimulates the ATPase activity of the core even in the absence of direct contacts between the RNA and core. To further corroborate this finding, we investigated the effect of a double-stranded RNA, formed by a self-complementary 14mer, that binds to the YxiN core (9) but not to the RRM. In the presence of this RNA, YxiN (both full-length and core) showed only background ATPase activity (Figure 3D). Thus, RNA that binds directly to the core but not to the RRM does not stimulate the intrinsic ATPase activity, confirming that RNA binding to the RRM is key for activation of the helicase core. We also tested the effect of the RRM on RNA unwinding, using a Cy5-labeled 32mer hybridized to a 9mer-Cy3 (32/9mer) as an unwinding substrate (8,28,44). The 9 bp duplex of the 32/9mer represents helix 91 of 23S rRNA. While YxiN_S108C/N444C readily unwound the 32/9mer in the presence of ATP, the isolated core exhibits no detectable unwinding activity under these conditions (Figure 3C). Altogether, these results suggest that the RRM is essential for efficient RNA binding, which triggers ATP hydrolysis and RNA unwinding by the core.

The peptide connecting the RecA_C to the RRM acts as a communication bridge

RNA binding to the RRM could be communicated to the helicase core in three ways: (i) through the RNA substrate that contacts both the RRM and the core, (ii) through direct interactions between the RRM and the core or (iii)

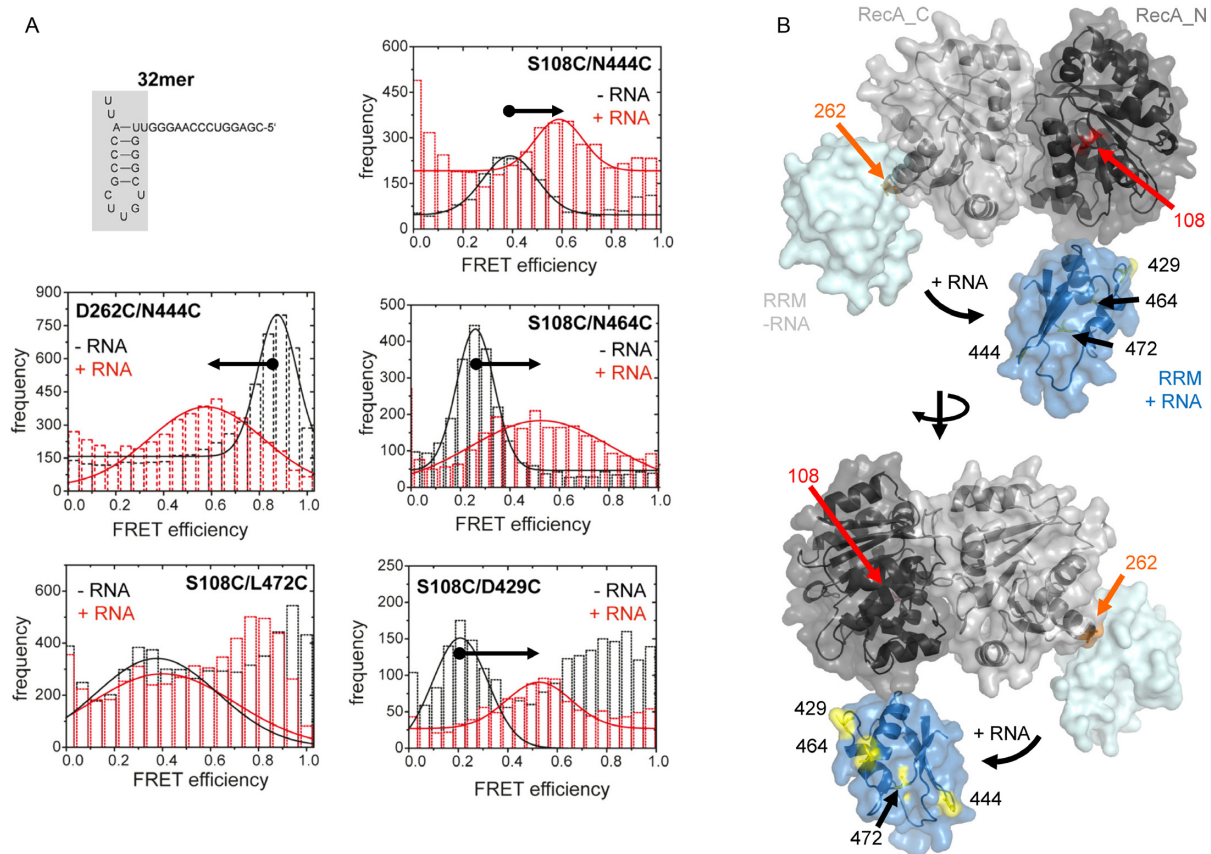


Figure 2. RNA binding induces movement of the RRM from a position next to the RecA_C to a position next to the RecA_N. (A) 32merRNA substrate (top left). The gray rectangle highlights hairpin 92 of 23S rRNA (32merHairpin). FRET histograms for YxiN_S108C/N444C, _D262C/N444C, _S108C/N464C, _S108C/D429C and _S108C/L472C in absence (black) and presence (red) of $1 \mu\text{M}$ 32mer RNA ($8 \mu\text{M}$ for YxiN_D262C/N444C because of its lower affinity for RNA). Arrows indicate changes in FRET efficiency upon RNA binding. (B) Structural model of YxiN in complex with 32mer RNA obtained by rigid-body docking of the RRM to the core using FRET distances as restraints. Top: front view, bottom: back view. The RRM position in the presence of RNA is shown in blue, otherwise the color code is the same as in Figure 1B.

through the linker connecting RecA_C with the RRM. We showed above that the 32merHairpin activates the ATP hydrolysis by the core without contacting it. Furthermore, the structural model for YxiN in the presence of RNA does not provide evidence for direct RRM/RecA contacts. The RRM cannot restore RNA-dependent ATPase activity of the core when supplied in *trans*, which is also pointing to a lack of extensive interactions between the RRM and the core (17). This leaves the linker (residues 361–400) between RecA_C and the RRM as the only possible communication bridge, although the mechanism of communication remains unclear. Secondary structure predictions by different algorithms that use position-specific scoring matrixes (PSIPRED (45)), combinations of evolutionary information and neural networks (PHD (46)), cascaded multiple classifiers (OUALI (47)) and the combination of sequence homology and structural homology (PSIPRED and SCRATCH (48)), consistently revealed a high propensity for the formation of two α -helices by the peptide (Figure 5; Supplementary Figure S2). In an extended conformation, these α -helices ($\sim 60 \text{ \AA}$ end-to-end distance) would be able to span the distance between the C-terminus of RecA_C and the N-terminus of the RRM both in the free and RNA-bound states (44 and 52 \AA , respectively). An α -helical con-

formation would restrict the positional freedom of the free and RNA-bound RRM relative to the core, and could facilitate communication of changes in the RRM position to the core. The linker between RecA_C and the RRM thus most likely acts as a communication bridge between the RRM and the active site for ATP hydrolysis and RNA unwinding.

The helicase core exhibits RNA-dependent conformational plasticity

The effect of RNA binding to the RRM on the ATPase activity of the core suggested an effect on core conformation. We therefore monitored conformational changes of the core upon RNA binding by smFRET with freely diffusing YxiN_S108C/S229C, labeled in RecA_N and RecA_C, and different types of RNA (Figure 6). YxiN_S108C/S229C has previously been employed to monitor RNA- and nucleotide-induced conformational changes of the YxiN core (7). Binding of the 32mer or the 32merHairpin to YxiN led to a decrease in E_{FRET} from ~ 0.60 to ~ 0.35 , pointing to a wider cleft between the RecA domains than in the ligand-free open state (Figure 6A and B). Subsequent addition of ADPNP to the YxiN/RNA complexes caused a further de-

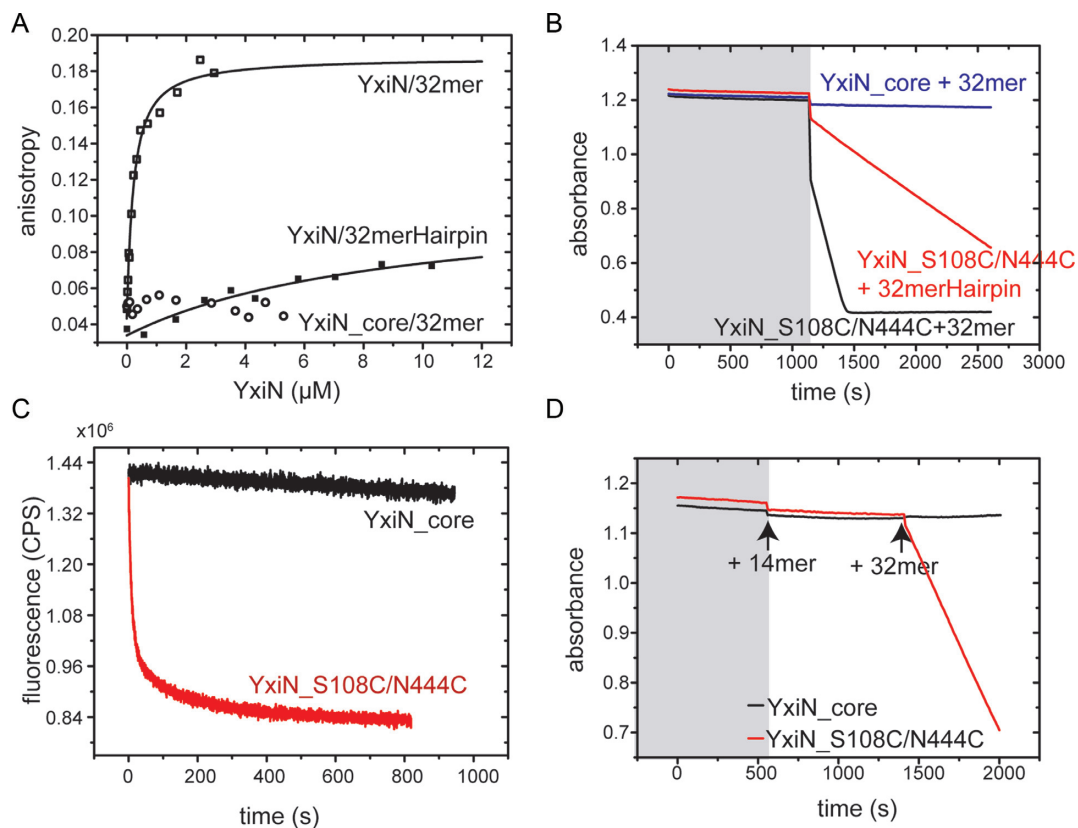


Figure 3. The RRM is required for RNA binding, ATPase activity and RNA unwinding. (A) Titration of 50 nM fluorescein-labeled 32mer or 32merHairpin in 50 mM Tris-HCl, pH 7.5, 150 mM NaCl, 5 mM MgCl₂ and 2 mM 2-mercaptoethanol with YxiN. The dissociation constants for the YxiN/32mer, YxiN/32merHairpin and YxiN_core/32mer (in the presence of 2 mM ADPNP) are $K_d = 0.17 \mu\text{M}$, $K_d = 7.0 \mu\text{M}$ and $K_d > 6 \mu\text{M}$, respectively. (B) ATP hydrolysis by 250 nM YxiN in the absence (gray background) and in the presence of RNA (white background), followed by a decrease in NADH absorbance in an enzyme-coupled assay in 50 mM Tris-HCl, pH 7.5, 150 mM NaCl, 5 mM MgCl₂ and 2 mM 2-mercaptoethanol with 5 mM ATP, 0.2 mM NADH, 0.4 mM phosphoenol pyruvate, 23 $\mu\text{g ml}^{-1}$ lactate dehydrogenase, 36 $\mu\text{g ml}^{-1}$ pyruvate kinase at 37°C. The RNA concentrations were 20 μM of 32mer (YxiN_S108C/N444C; black), 40 μM of 32merHairpin RNA (YxiN_S108C/N444C; red) or 40 μM of 32mer (YxiN_core; blue). The ATP hydrolysis rates are $k_{\text{hyd}} = 1.24 \pm 0.04 \text{ ATP YxiN}^{-1} \text{ s}^{-1}$, $k_{\text{hyd}} = 0.20 \pm 0.04 \text{ ATP YxiN}^{-1} \text{ s}^{-1}$ and $k_{\text{hyd}} = 2.4 (\pm 0.4) \times 10^{-3} \text{ ATP YxiN}^{-1} \text{ s}^{-1}$, respectively. Experiments were performed in triplicates. (C) Unwinding of 0.5 μM Cy5-32mer/9mer-Cy3 hybridized RNA in 50 mM Tris-HCl, pH 7.5, 150 mM NaCl, 5 mM MgCl₂ and 2 mM 2-mercaptoethanol by YxiN_S108C/N444C in the presence of 5 mM ATP, followed by a decrease in acceptor fluorescence. YxiN rapidly unwinds the 32/9mer, whereas YxiN_core does not show detectable RNA unwinding activity. The unwinding experiments were conducted in the presence of 5 μM unlabeled trap RNA that is complementary to the 9mer (single turnover conditions). (D) ATP hydrolysis by 250 nM YxiN_core or YxiN_S108C/N444C in absence and presence of 14mer dsRNA (10 μM) and 32mer RNA (5 μM). Experiments were conducted in duplicates.

crease in FRET ($E_{\text{FRET}} \sim 0.25$). Both RNAs thus affect the conformation of the core similarly. In contrast, binding of the 154mer RNA alone to YxiN caused little changes of the FRET efficiency, but higher E_{FRET} , consistent with core closure, was observed upon subsequent addition of ADPNP (Figure 6C), in accordance with previous observations (7). The conformational space of the helicase core thus depends on the identity of the RNA that is bound to the RRM.

YxiN species with widened inter-domain clefts represent off-pathway intermediates

According to the current model of RNA unwinding by DEAD-box proteins, helicase activity requires cycling of the helicase core between open and closed states (7,31). The 154mer stimulates the ATPase activity of YxiN and increases the fraction of the helicase core in the closed state (7). The 32mer or 32merHairpin both stimulate ATPase activity, yet no high FRET states are observed, suggesting that these are most likely populated only transiently.

To comprehensively explore the conformational space of the core, we conducted TIRF experiments on N-terminally biotinylated YxiN_A115C/S229C, labeled with Alexa555 (donor) and Alexa647 (acceptor) dyes and immobilized on streptavidin-functionalized microscope cover slips. Donor-acceptor-labeled YxiN_A115C/S229C reports on RNA- and nucleotide-induced conformational changes of the YxiN core (7,8). TIRF experiments were performed in the absence and presence of 32mer, 154mer, ADPNP or ATP (Figure 7). Representative fluorescence and FRET trajectories for YxiN and YxiN/32mer/ATP are shown in Supplementary Figure S3. Histograms of the FRET efficiencies for each molecule at the beginning of the experiment (35) (during the first three seconds) provide an overview about the populated states (Figure 7). In the absence of ligands, FRET histograms for YxiN (Figure 7A) show a main peak with $E_{\text{FRET}} \sim 0.34$, with a shoulder at $E_{\text{FRET}} \sim 0.45$, consistent with an open conformation of the helicase core and in agreement with previous results (8). The FRET

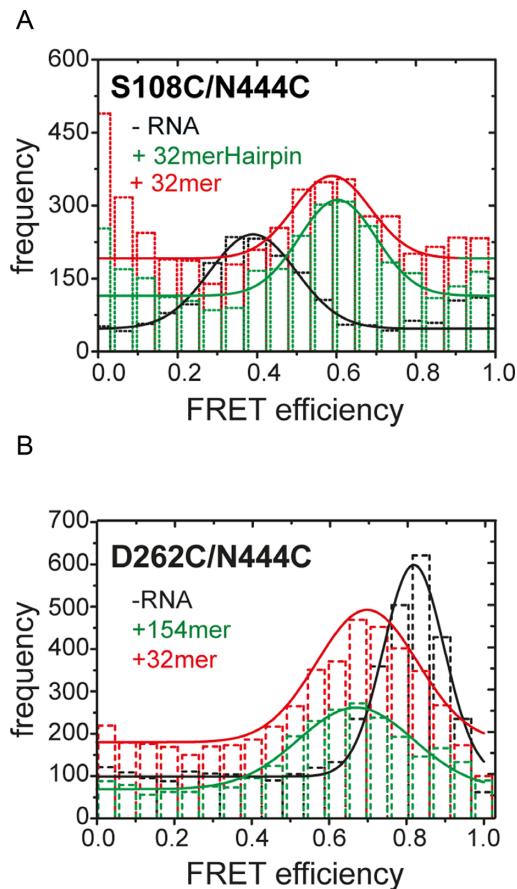


Figure 4. Different RNAs containing hairpin 92 induce the same positional shift of the RRM. (A) FRET histograms for YxiN_S108C/N444C in the absence (black) and presence of the 32mer (1 μ M; red) and the 32merHairpin (15 μ M; green) that lacks the 5'-single-stranded extension. (B) FRET histograms for YxiN_D262C/N444C in the absence of RNA (black), in presence of 32mer RNA (red) and in presence of 154mer RNA (green).

efficiencies are independent of bin size (Supplementary Figure S4). FRET histograms of YxiN/154mer/ADPNP (Figure 7B) show a predominant state with $E_{\text{FRET}} \sim 0.40$, corresponding to the initial open state and high FRET states ($E_{\text{FRET}} \sim 0.60$ and ~ 0.70) indicative of the functional closed state (7) that are less populated than observed previously for YxiN in solution (8). In contrast, histograms for YxiN/32mer/ADPNP and YxiN/32mer/ATP complexes (Figure 7C and D) showed a predominant low FRET state ($E_{\text{FRET}} 0.20\text{--}0.30$, 'wide-open'), smaller populations of medium FRET ($E_{\text{FRET}} \sim 0.50\text{--}0.60$) and high FRET states ($E_{\text{FRET}} \geq 0.60$) that most likely reflect the functional closed state. Non-idealized FRET histograms simply show a shift to low FRET (Supplementary Figure S5) because of fluorescence fluctuations (Supplementary Figure S3), in agreement with confocal data (Figure 6). The YxiN/32mer complex in the absence of nucleotides (Figure 7E) is predominantly in the open state ($E_{\text{FRET}} \sim 0.35$), with a subpopulation at higher FRET ($E_{\text{FRET}} \sim 0.60$). The FRET histograms are in qualitative agreement with FRET changes observed in confocal experiments (Figure 6), namely population of

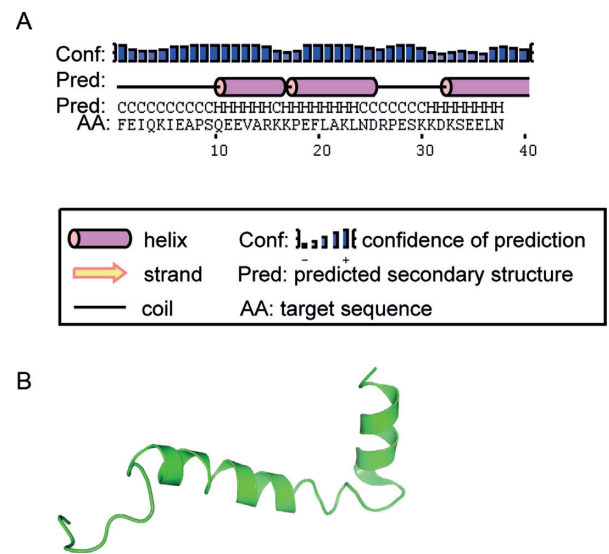


Figure 5. The peptide connecting the RecA_C to the RRM has a propensity to form an α -helical structure. (A) Secondary structure prediction performed on the peptide sequence connecting RecA_C and the RRM by PSIPRED shows very high propensity to adopt two α -helices. Other prediction algorithms gave similar results. (B) Model of the α -helical structure of the RecA_C-RRM peptide.

high FRET states in presence of the 154mer and ADPNP, and shifts to lower FRET with the 32mer and ADPNP.

To analyze the dynamic behavior of YxiN across the entire time trajectory (~ 180 s), we generated FDPs that reflect the molecules that remain in the same FRET state throughout the observation time, and TDPs that measure the inter-conversion between individual states (Figure 7). The largest error in the determination of FRET efficiencies from FDPs or TDPs is 0.02 (half-width of the peak in the FDP of YxiN in absence of ligands; Figure 7A). Thus, FRET states with differences in $E_{\text{FRET}} > 0.02$ are considered different states.

For YxiN, 48% of the 184 molecules remained in the same FRET state (~ 0.37 or ~ 0.45 , Figure 7A). The other 52% inter-converted between these two states (~ 0.33 or ~ 0.45). In contrast to free YxiN, all RNA- and nucleotide-complexes showed less conformational fluctuations, with 60–90% of the molecules remaining in the same FRET state throughout the measurement. In the YxiN/154mer/ADPNP complex, 73% of the 80 molecules analyzed remained in one state with $E_{\text{FRET}} \sim 0.40$ (open (7,8)) throughout the experiment. In addition, species with E_{FRET} of ~ 0.47 , ~ 0.55 , ~ 0.60 and ~ 0.65 and minor populations of states with $E_{\text{FRET}} \sim 0.33$ and ~ 0.78 E_{FRET} (closed (7,8)) were also observed (Figure 7B). The TDP for the 27% interconverting molecules reveals transitions between $E_{\text{FRET}} \sim 0.70$ (closed) and ~ 0.42 (open), ~ 0.70 (closed) and ~ 0.52 and ~ 0.42 (open) and ~ 0.29 (Figure 7B). The state with intermediate E_{FRET} of ~ 0.52 exchanges with the functional ~ 0.70 state and is likely a low-populated intermediate. States with intermediate FRET efficiencies (0.45–0.65) have been observed previously for YxiN variants with mutations in the interface that is formed between the RecA domains in the closed state (8), and may correspond to YxiN molecules where the inter-domain cleft is not completely

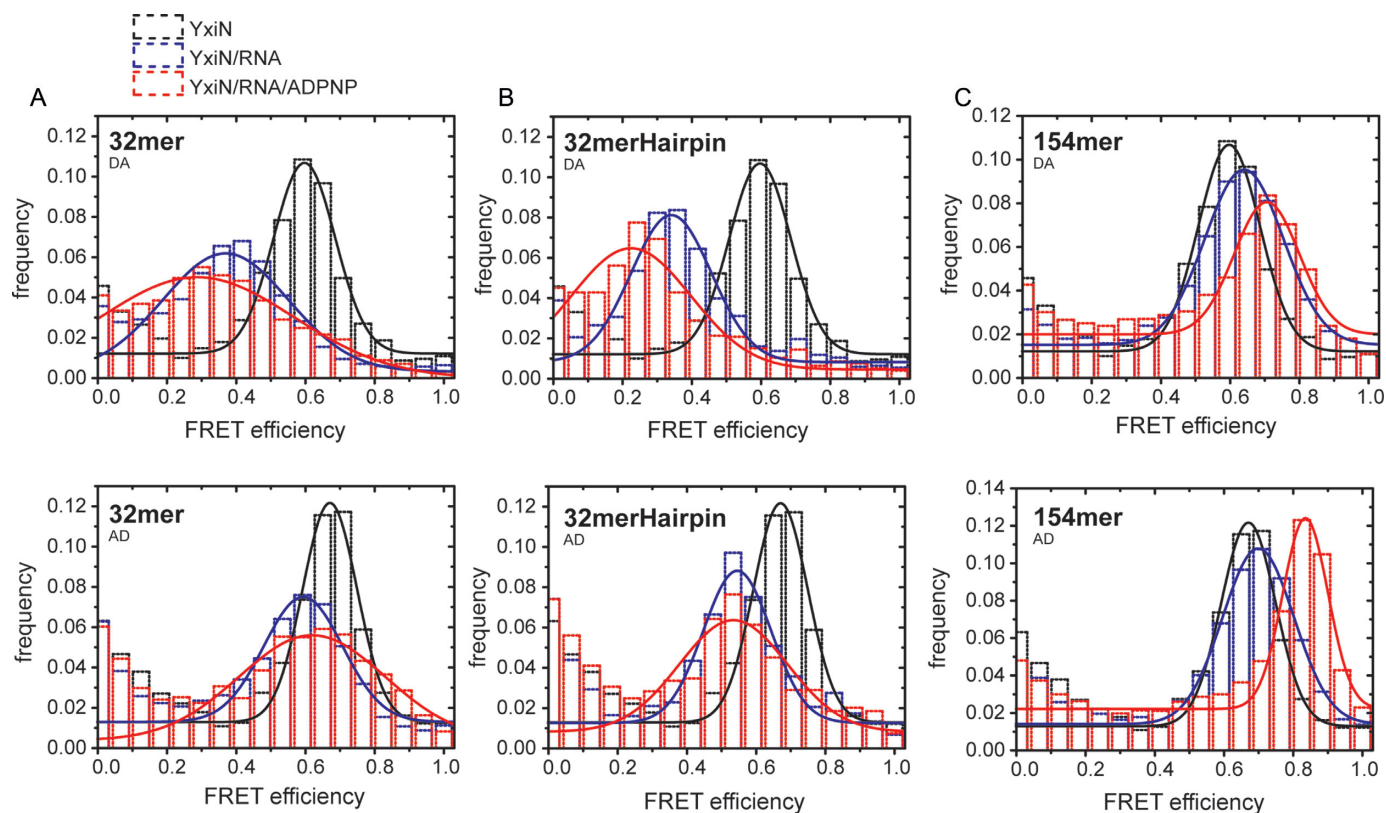


Figure 6. The 32mer and 32merHairpin promote a low FRET conformation of the YxiN core. (A) FRET histograms of ~ 200 pM YxiN_S108C/S229C (black), YxiN/32mer complex ($2.0 \mu\text{M}$ of 32mer, blue) and YxiN/32mer/ADPNP complex ($2.0 \mu\text{M}$ of 32mer and 5 mM ADPNP, red) in 50 mM Tris-HCl, pH 7.5, 150 mM NaCl, 5 mM MgCl_2 , 2 mM 2-mercaptoethanol, at room temperature ($\sim 23^\circ\text{C}$). (B) The same as in (A) but with $5.0 \mu\text{M}$ 32merHairpin RNA. (C) The same as in (A) but with $0.4 \mu\text{M}$ 154mer RNA. The photophysical properties of the dyes differ slightly depending on their attachment site, which leads to differences in correction factors, and different FRET efficiencies for the DA (S108C-A488/S229C-A546) and AD (S108C-A546/S229C-A488) configurations. The two histograms shown are analyzed for each configuration (DA, top, AD, bottom). The lines are fits of Gaussian distributions to the data.

closed. The state with $E_{\text{FRET}} \sim 0.29$ that interconverts with the open state represents a low-populated (wide-)open state.

For the YxiN/32mer complex, 81% of the 284 molecules remained in the same state, predominantly in the initial open state ($E_{\text{FRET}} \sim 0.40$, Figure 7C). A smaller population spreads toward lower E_{FRET} (~ 0.30), in agreement with the shift to lower FRET efficiencies observed by confocal microscopy. The 19% interconverting molecules mostly switched between the open state ($E_{\text{FRET}} \sim 0.38$) and a high $E_{\text{FRET}} \sim 0.68$ state (Figure 7C) that is not significantly populated in equilibrium and therefore not detected by confocal microscopy.

For the YxiN/32mer/ADPNP complex, nearly all molecules (55 of 61, 90%) remain in the same FRET state throughout the experiment. The FDP shows states of $E_{\text{FRET}} \sim 0.30$, 0.36 and 0.67 (Figure 7D), with the state of $E_{\text{FRET}} \sim 0.30$ being much more populated than the rest. Because of the low number of interconverting molecules ($n = 6$), a TDP plot is not statistically relevant.

In the presence of 32mer and ATP instead of the non-hydrolyzable ADPNP, 60% of 194 molecules are non-interconverting. Most are trapped in a state of $E_{\text{FRET}} \sim 0.30$, in agreement with the observed shift to lower FRET in the histograms, while some have an E_{FRET} of ~ 0.37 , (Figure 7E). The remaining 40% of the molecules undergo

four types of transitions: a predominant inter-conversion of states with $E_{\text{FRET}} \sim 0.38$ (open) and ~ 0.24 (wide-open), transitions between ~ 0.52 (intermediate) and ~ 0.33 (open), between ~ 0.76 (closed) and ~ 0.55 (intermediate) and some transitions between $E_{\text{FRET}} \sim 0.62$ and ~ 0.44 (open). The largest number of transitions involves the species with $E_{\text{FRET}} \sim 0.24$, which does not link with the functional high FRET state, and therefore represents an off-pathway intermediate (wide-open \rightarrow open \rightarrow closed; in contrast to a sequence of open \rightarrow wide-open \rightarrow closed that would be observed for an on-pathway intermediate). A summary of the observed conformational states and their interconversion is shown in Supplementary Figure S6.

In summary, binding of the 154mer RNA to YxiN in the presence of nucleotide predominantly favors high FRET (closed) states. In contrast, binding of the 32mer leads to low FRET species with a wider inter-domain cleft that are off-pathway, and to the transient population of high FRET states, which rationalizes the observed stimulation of ATPase activity by these RNAs.

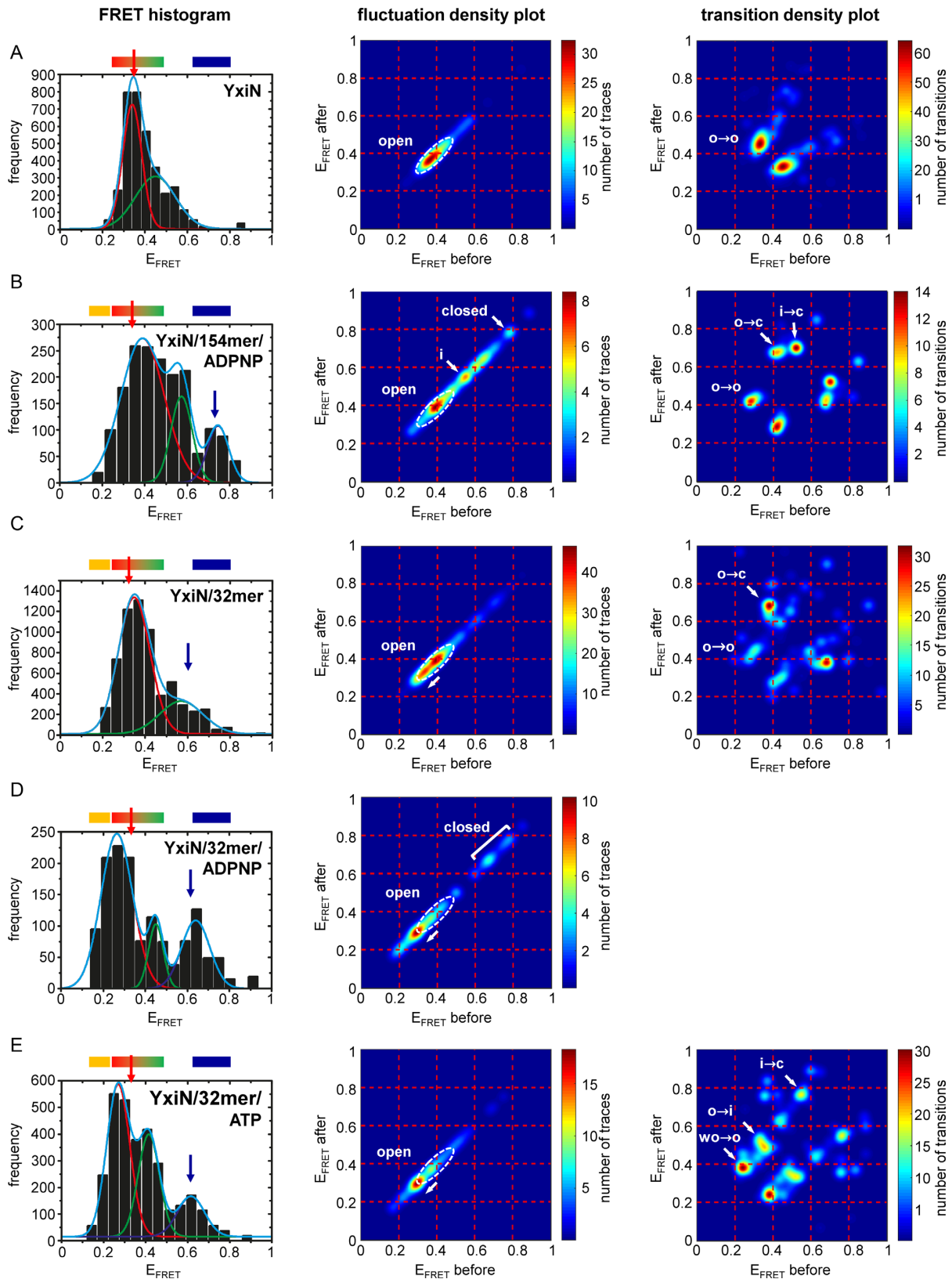


Figure 7. The low FRET states of the core are off-pathway intermediates. Idealized FRET histograms from smFRET experiments by TIRF microscopy (left), fluctuation density plots (FDP, center), and transition density plots (TDP, right) of Alexa555/Alexa647-labeled N-terminal biotinylated YxiN_A115C/S229C in 50 mM Tris-HCl, pH 7.5, 150 mM NaCl, 5 mM MgCl₂, 0.5 μM YxiN RecA_N, 2 mM 2-mercaptoethanol in the absence and presence of RNA (32mer or 154mer) and/or nucleotide (ATP or ADPNP). (A) YxiN; $n_{\text{tot}} = 184$, $n_{\text{FDP}} = 88$, $n_{\text{TDP}} = 96$, (B) YxiN/154mer/ADPNP; $n_{\text{tot}} = 80$, $n_{\text{FDP}} = 58$, $n_{\text{TDP}} = 22$, (C) YxiN/32mer; $n_{\text{tot}} = 284$, $n_{\text{FDP}} = 230$, $n_{\text{TDP}} = 54$, (D) YxiN/32mer/ADPNP; $n_{\text{tot}} = 61$, $n_{\text{FDP}} = 55$, $n_{\text{TDP}} = 6$ (n.a.), (E) YxiN/32mer/ATP; $n_{\text{tot}} = 600$, $n_{\text{FDP}} = 150$, $n_{\text{TDP}} = 150$.

RNA binding to the RRM allosterically activates the helicase core

Our smFRET experiments show that RNA binding to the RRM leads to a shift in its position, and to changes in the conformational space that is accessible to the helicase core. In conjunction with ATPase and RNA unwinding experiments, these findings point to an allosteric activation of the helicase core upon RNA binding to the RRM. We tested this hypothesis by performing unwinding experiments with a 15/9mer that corresponds to the 32/9mer lacking the hairpin. An allosteric activation mechanism would predict that addition of the 32merHairpin and its binding to the RRM should stimulate unwinding of the 15/9mer. YxiN unwinds the isolated 15/9mer slowly, with a rate constant of $k_{\text{unwind}} = 0.003 \text{ s}^{-1}$ (Figure 8). In the context of the 32/9mer, unwinding is 8-fold faster, with a rate constant of $k_{\text{unwind}} = 0.024 \text{ s}^{-1}$. In presence of the 32merHairpin, unwinding of the 15/9mer is accelerated 2.5-fold ($k_{\text{unwind}} = 0.007 \text{ s}^{-1}$) compared to unwinding of the isolated 15/9mer. Thus, binding of the 32merHairpin, the associated movement of the RRM and the changes in the conformational dynamics of the helicase core indeed lead to an activation of the helicase core, with the RNA bound to the RRM acting as an allosteric activator.

DISCUSSION

RNA binding to the RRM alters the position of the RRM

We have shown that the C-terminal RRM of YxiN is located in defined positions relative to the core, and moves from a position close to RecA_C in the absence of RNA to the proximity of RecA_N in the RNA-bound state. The movement is driven by RNA binding to the RRM and does not require interactions of the bound RNA with the core. Nevertheless, RNA binding to the RRM affects the core: the conformation of the core is modulated, and its RNA-dependent ATPase and RNA unwinding activities are stimulated.

Communication between the RNA binding site of the RRM and the active site of the core

The current model on the activation of ATP hydrolysis by RNA is based entirely on motifs identified within the core that mediate ATPase activity (3,49,4). RNA binding domains flanking the core were believed to function as passive anchors that mediate high affinity binding to defined elements in the RNA substrate, and the helicase core can then unwind nearby RNA duplexes (18,50). Our results now show that binding of the YxiN RRM to the RNA not only anchors the helicase on the RNA, but also modulates the

core conformation and its ATPase and RNA unwinding activities, demonstrating that RNA binding at the RRM is communicated to the core. This communication does not require binding of the RNA recognized by the RRM to the core, which excludes an RNA-mediated interaction of core and RRM. In the RNA-bound state, the RRM is located next to the RecA_N. RecA_N contains most of the conserved motifs for ATP binding and hydrolysis, and it would be conceivable that the RNA-bound RRM stimulates RNA-dependent ATPase activity by affecting the conformation of these motifs. However, the structural models for YxiN in the presence of RNA do not point to extensive interactions between core and RRM. In addition, the isolated RRM cannot restore RNA-dependent ATPase activity of the core when supplied *trans*, which is also pointing to a lack of extensive interactions between the RRM and the core (17). The peptide connecting the RecA_C to the RRM has a high propensity for α -helix formation, and the end-to-end distance of such an extended α -helical peptide is sufficient to traverse the distance separating the RecA_C and the RRM. The linker therefore most likely acts as a direct communication bridge between RRM and core, and mediates the allosteric activation of core activities.

RNA binding to the RRM and core conformation

Binding of RNA to the RRM modulates the conformation of the helicase core. Switching of the core between open and closed states has been linked to RNA-dependent ATPase- and ATP-dependent RNA unwinding activities of the core (6–8,31). However, instead of observing high FRET species in presence of the 32mer and 32merHairpin, species with lower FRET appeared, representing conformations of the core with increased separation of the two RecA domains. High FRET states, although not populated in equilibrium (i.e. absent in FRET histograms from confocal experiments (Figure 6) and in FDPs from TIRF experiments; Figure 7), are formed transiently (evident in TDPs; Figure 7), in agreement with the observed increase in ATPase activity upon binding of these RNAs. From the lack of interchange between low FRET species and the functional high FRET state in the presence of ATP, we conclude that the low FRET states induced by binding of the 32mer or the 32merHairpin to the RRM are off-pathway intermediates that are only accessed from the open state of the core. In contrast, binding of the 154mer RNA (in the presence of ADPNP) favors population of the high FRET functional state of the core. Thus, the core can adapt to the type of RNA bound by conformational plasticity. For its role in ribosome biogenesis (51) YxiN needs to distinguish unproductive assembly intermediates from functional, native ribosomes. The different level of activation of the core by the 154mer and the smaller 32mer RNA may reflect the differential recognition

(E) YxiN/32mer/ATP; $n_{\text{tot}} = 194$, $n_{\text{FDP}} = 116$, $n_{\text{TDP}} = 78$. Experiments were performed at room temperature. The concentrations were $<30 \text{ pM}$ YxiN, $15 \mu\text{M}$ of the 32mer RNA, $1 \mu\text{M}$ of the 154mer RNA, 20 mM ATP or 10 mM ADPNP. The FRET histograms show the states populated within the first three seconds. The red arrow indicates an open state of the core, the blue arrow marks the closed state. The colored bars above the histogram indicate FRET ranges for wide-open (orange), open (red), intermediate (green) and closed states (blue). Fluctuation and transition density plots (FDPs, TDPs) show fluctuations and transitions across the entire trajectory (upto 180 s). The white arrow in the FDPs indicates shifts from the open state toward lower FRET states. o: open conformation, c: closed conformation, i: intermediate, wo: wide-open, low FRET state; n_{tot} : total number of molecules observed, n_{FDP} : number of static molecules, n_{TDP} : number of dynamic molecules inter-converting between different conformational states, n.a.: not analyzed.

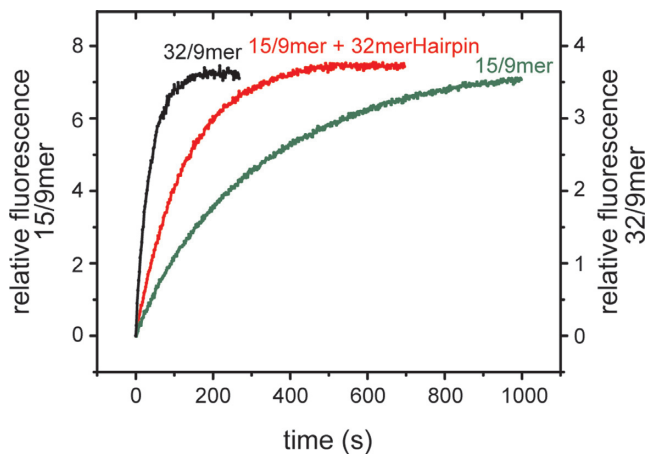


Figure 8. Binding of RNA to the RRM allosterically activates unwinding by the helicase core. Unwinding of 0.5 μM FAM-32mer/9mer-Cy3 RNA (black) and 0.5 μM FAM-15mer/9mer-Cy3 RNA in the absence (green) and presence (red) of 5 μM 32merHairpin by YxiN_{N444C} in 50 mM Tris-HCl, pH 7.5, 150 mM NaCl, 5 mM MgCl₂, 2 mM 2-mercaptoethanol and 5 mM ATP, followed by the increase in donor fluorescence. YxiN rapidly unwinds the duplex of the 32/9mer ($k_{\text{unwind}} = 0.024 \text{ s}^{-1}$). The 15/9mer is unwound very slowly ($k_{\text{unwind}} = 0.003 \text{ s}^{-1}$). In the presence of 32merHairpin, unwinding of the 15/9mer is accelerated 2.5-fold, to $k_{\text{unwind}} = 0.007 \text{ s}^{-1}$. The unwinding experiments were conducted in the presence of 5 μM unlabeled trap RNA that is complementary to the 9mer (single turnover conditions).

of these elements in their distinct structural contexts. The effect of RNA binding to the RRM on the conformational space of the core, the dominant populations and their interchange are tightly linked to the ATPase and unwinding activities of the core. Our results therefore show that the YxiN RRM is not a passive RNA anchor but undergoes an RNA-induced movement that is communicated to the core and modulates core activity. Allosteric regulation of core activities by RNA; mediated through an RNA-induced movement of ancillary domains, may constitute a general regulatory mechanism of DEAD-box proteins.

SUPPLEMENTARY DATA

Supplementary Data are available at NAR Online.

ACKNOWLEDGEMENTS

This project was funded by the DFG (KL1153/7-1). The authors thank Ulf Harms for assistance with the functionalization of microscope slides, Jessica Guddorf for excellent technical assistance, and Airat Gubaev for helpful discussions.

FUNDING

DFG [KL1153/7-1]. The open access publication charge for this paper has been waived by Oxford University Press - NAR Editorial Board members are entitled to one free paper per year in recognition of their work on behalf of the journal.

Conflict of interest statement. None declared.

REFERENCES

- Putnam, A.A. and Jankowsky, E. (2013) DEAD-box helicases as integrators of RNA, nucleotide and protein binding. *Biochim. Biophys. Acta*, **1829**, 884–893.
- Henn, A., Bradley, M.J. and De La Cruz, E.M. (2012) ATP utilization and RNA conformational rearrangement by DEAD-Box proteins. *Annu. Rev. Biophys.*, **41**, 247–267.
- Hilbert, M., Karow, A.R. and Klostermeier, D. (2009) The mechanism of ATP-dependent RNA unwinding by DEAD box proteins. *Biol. Chem.*, **390**, 1237–1250.
- Gorbalenya, A.E. and Koonin, E.V. (1993) Helicases: amino acid sequence comparisons and structure-function relationships. *Curr. Opin. Struct. Biol.*, **3**, 419–429.
- Cordin, O., Banroques, J., Tanner, N.K. and Linder, P. (2006) The DEAD-box protein family of RNA helicases. *Gene*, **367**, 17–37.
- Sengoku, T., Nureki, O., Nakamura, A., Kobayashi, S. and Yokoyama, S. (2006) Structural basis for RNA unwinding by the DEAD-Box protein drosophila vasa. *Cell*, **125**, 287–300.
- Theissen, B., Karow, A.R., Kohler, J., Gubaev, A. and Klostermeier, D. (2008) Cooperative binding of ATP and RNA induces a closed conformation in a DEAD box RNA helicase. *Proc. Natl. Acad. Sci. U.S.A.*, **105**, 548–553.
- Karow, A.R. and Klostermeier, D. (2009) A conformational change in the helicase core is necessary but not sufficient for RNA unwinding by the DEAD box helicase YxiN. *Nucleic Acids Res.*, **37**, 4464–4471.
- Samatanga, B. and Klostermeier, D. (2014) DEAD-box RNA helicase domains exhibit a continuum between complete functional independence and high thermodynamic coupling in nucleotide and RNA duplex recognition. *Nucleic Acids Res.*, **42**, 10644–10654.
- Collins, R., Karlberg, T., Lehtio, L., Schutz, P., van den Berg, S., Dahlgren, L.G., Hammarstrom, M., Weigelt, J. and Schuler, H. (2009) The DExD/H-box RNA helicase DDX19 is regulated by an alpha-helical switch. *J. Biol. Chem.*, **284**, 10296–10300.
- Fan, J.S., Cheng, Z., Zhang, J., Noble, C., Zhou, Z., Song, H. and Yang, D. (2009) Solution and Crystal Structures of mRNA Exporter Dbp5p and Its Interaction with Nucleotides. *J. Mol. Biol.*, **388**, 1–10.
- Fuller-Pace, F.V., Nicol, S.M., Reid, A.D. and Lane, D.P. (1993) DbpA: a DEAD box protein specifically activated by 23s rRNA. *EMBO J.*, **12**, 3619–3626.
- Nicol, S.M. and Fuller-Pace, F.V. (1995) The 'DEAD box' protein DbpA interacts specifically with the peptidyltransferase center in 23S rRNA. *Proc. Natl. Acad. Sci. U.S.A.*, **92**, 11681–11685.
- Pugh, G.E., Nicol, S.M. and Fuller-Pace, F.V. (1999) Interaction of the *Escherichia coli* DEAD box protein DbpA with 23 S ribosomal RNA. *J. Mol. Biol.*, **292**, 771–778.
- Diges, C.M. and Uhlenbeck, O.C. (2001) *Escherichia coli* DbpA is an RNA helicase that requires hairpin 92 of 23S rRNA. *EMBO J.*, **20**, 5503–5512.
- Kossen, K., Karginov, F.V. and Uhlenbeck, O.C. (2002) The carboxy-terminal domain of the DExDH protein YxiN is sufficient to confer specificity for 23S rRNA. *J. Mol. Biol.*, **324**, 625–636.
- Karginov, F.V., Caruthers, J.M., Hu, Y., McKay, D.B. and Uhlenbeck, O.C. (2005) YxiN is a modular protein combining a DEx(D/H) core and a specific RNA-binding domain. *J. Biol. Chem.*, **280**, 35499–35505.
- Mallam, A.L., Jarmoskaite, I., Tijerina, P., Del Campo, M., Seifert, S., Guo, L., Russell, R. and Lambowitz, A.M. (2011) Solution structures of DEAD-box RNA chaperones reveal conformational changes and nucleic acid tethering by a basic tail. *Proc. Natl. Acad. Sci. U.S.A.*, **108**, 12254–12259.
- Mohr, G., Del Campo, M., Mohr, S., Yang, Q., Jia, H., Jankowsky, E. and Lambowitz, A.M. (2008) Function of the C-terminal domain of the DEAD-Box protein Mss116p analyzed in vivo and in vitro. *J. Mol. Biol.*, **375**, 1344–1364.
- Tijerina, P., Bhaskaran, H. and Russell, R. (2006) Nonspecific binding to structured RNA and preferential unwinding of an exposed helix by the CYT-19 protein, a DEAD-box RNA chaperone. *Proc. Natl. Acad. Sci. U. S. A.*, **103**, 16698–16703.
- Del Campo, M. and Lambowitz, A.M. (2009) Structure of the yeast DEAD-box protein Mss116p reveals two wedges that crimp RNA. *Mol. Cell*, **35**, 598–609.
- Napetschnig, J., Kassube, S.A., Debler, E.W., Wong, R.W., Blobel, G. and Hoelz, A. (2009) Structural and functional analysis of the

- interaction between the nucleoporin Nup214 and the DEAD-box helicase Ddx19. *Proc. Natl. Acad. Sci. U.S.A.*, **106**, 3089–3094.
23. Rudolph, M.G. and Klostermeier, D. (2015) When core competence is not enough: functional interplay of the DEAD-box helicase core with ancillary domains and auxiliary factors in RNA binding and unwinding. *Biol. Chem.*, **396**, 849–865.
 24. Kossen, K. and Uhlenbeck, O.C. (1999) Cloning and biochemical characterization of *Bacillus subtilis* YxiN, a DEAD protein specifically activated by 23S rRNA: delineation of a novel sub-family of bacterial DEAD proteins. *Nucleic Acids Res.*, **27**, 3811–3820.
 25. Martin, R., Straub, A.U., Doebele, C. and Bohnsack, M.T. (2012) DExD/H-box RNA helicases in ribosome biogenesis. *RNA Biol.*, **9**, 1173–1182.
 26. Karow, A.R., Theissen, B. and Klostermeier, D. (2007) Authentic interdomain communication in an RNA helicase reconstituted by expressed protein ligation of two helicase domains. *FEBS J.*, **274**, 463–473.
 27. Harms, U., Andreou, A.Z., Gubaev, A. and Klostermeier, D. (2014) eIF4B, eIF4G and RNA regulate eIF4A activity in translation initiation by modulating the eIF4A conformational cycle. *Nucleic Acids Res.*, **42**, 7911–7922.
 28. Karow, A.R. and Klostermeier, D. (2010) A structural model for the DEAD box helicase YxiN in solution: localization of the RNA-binding domain. *J. Mol. Biol.*, **402**, 629–637.
 29. Aregger, R. and Klostermeier, D. (2009) The DEAD-box helicase YxiN maintains a closed conformation during ATP hydrolysis. *Biochemistry*, **48**, 10679–10681.
 30. Adam, H. (1962) *Methoden der enzymatischen Analyse*. Bergmeyer, H.U. (Hrsg.), Verlag Chemie, Weinheim pp. 573–577.
 31. Andreou, A.Z. and Klostermeier, D. (2012) Conformational changes of DEAD-Box helicases monitored by single molecule fluorescence resonance energy transfer. *Methods Enzymol.*, **511**, 75–109.
 32. Parker, C.A. and Rees, W.T. (1960) Correction of Fluorescence Spectra and Measurement of Fluorescence Quantum Efficiency. *Analyst*, **85**, 587–600.
 33. Magde, D., Wong, R. and Seybold, P.G. (2002) Fluorescence quantum yields and their relation to lifetimes of rhodamine 6G and fluorescein in nine solvents: improved absolute standards for quantum yields. *Photochem. Photobiol.*, **75**, 327–334.
 34. Kalinin, S., Peulen, T., Sindbert, S., Rothwell, P.J., Berger, S., Restle, T., Goody, R.S., Gohlke, H. and Seidel, C.A. (2012) A toolkit and benchmark study for FRET-restrained high-precision structural modeling. *Nat. Methods*, **9**, 1218–1225.
 35. Ha, T., Ting, A.Y., Liang, J., Caldwell, W.B., Deniz, A.A., Chemla, D.S., Schultz, P.G. and Weiss, S. (1999) Single-molecule fluorescence spectroscopy of enzyme conformational dynamics and cleavage mechanism. *Proc. Natl. Acad. Sci. U.S.A.*, **96**, 893–898.
 36. Bronson, J.E., Fei, J., Hofman, J.M., Gonzalez, R.L. Jr and Wiggins, C.H. (2009) Learning rates and states from biophysical time series: a Bayesian approach to model selection and single-molecule FRET data. *Biophys. J.*, **97**, 3196–3205.
 37. McKinney, S.A., Joo, C. and Ha, T. (2006) Analysis of single-molecule FRET trajectories using Hidden Markov modeling. *Biophys. J.*, **91**, 1941–1951.
 38. Story, R.M., Li, H. and Abelson, J.N. (2001) Crystal structure of a DEAD box protein from the hyperthermophile *Methanococcus jannaschii*. *Proc. Natl. Acad. Sci. U.S.A.*, **98**, 1465–1470.
 39. Muschielok, A., Andrecka, J., Jawhari, A., Bruckner, F., Cramer, P. and Michaelis, J. (2008) A nano-positioning system for macromolecular structural analysis. *Nat. Methods*, **5**, 965–971.
 40. Muschielok, A. and Michaelis, J. (2011) Application of the nano-positioning system to the analysis of fluorescence resonance energy transfer networks. *J. Phys. Chem. B*, **115**, 11927–11937.
 41. Wang, S., Overgaard, M.T., Hu, Y. and McKay, D.B. (2007) The *Bacillus subtilis* RNA Helicase YxiN is distended in solution. *Biophys. J.*, **94**, L01–L03.
 42. Hardin, J.W., Hu, Y.X. and McKay, D.B. (2010) Structure of the RNA binding domain of a DEAD-box helicase bound to its ribosomal RNA target reveals a novel mode of recognition by an RNA recognition motif. *J. Mol. Biol.*, **402**, 412–427.
 43. Tsu, C.A., Kossen, K. and Uhlenbeck, O.C. (2001) The *Escherichia coli* DEAD protein DbpA recognizes a small RNA hairpin in 23S rRNA. *RNA*, **7**, 702–709.
 44. Steimer, L., Wurm, J.P., Linden, M.H., Rudolph, M.G., Wohnert, J. and Klostermeier, D. (2013) Recognition of two distinct elements in the RNA substrate by the RNA binding domain of the *T. thermophilus* DEAD box helicase Hera. *Nucleic Acids Res.*, **41**, 6259–6272.
 45. Jones, D.T. (1999) Protein secondary structure prediction based on position-specific scoring matrices. *J. Mol. Biol.*, **292**, 195–202.
 46. Rost, B., Sander, C. and Schneider, R. (1994) PHD—an automatic mail server for protein secondary structure prediction. *Comput. Appl. Biosci.*, **10**, 53–60.
 47. Ouali, M. and King, R.D. (2000) Cascaded multiple classifiers for secondary structure prediction. *Protein Sci.*, **9**, 1162–1176.
 48. Cheng, J., Randall, A.Z., Sweredoski, M.J. and Baldi, P. (2005) SCRATCH: a protein structure and structural feature prediction server. *Nucleic Acids Res.*, **33**, W72–W76.
 49. Jankowsky, E. (2011) RNA helicases at work: binding and rearranging. *Trends Biochem. Sci.*, **36**, 19–29.
 50. Mallam, A.L., Del Campo, M., Gilman, B., Sidote, D.J. and Lambowitz, A.M. (2012) Structural basis for RNA-duplex recognition and unwinding by the DEAD-box helicase Mss116p. *Nature*, **490**, 121–125.
 51. Sharpe Elles, L.M., Sykes, M.T., Williamson, J.R. and Uhlenbeck, O.C. (2009) A dominant negative mutant of the *E. coli* RNA helicase DbpA blocks assembly of the 50S ribosomal subunit. *Nucleic Acids Res.*, **37**, 6503–6514.